Energy for Sustainable Development 31 (2016) 108–117

Contents lists available at ScienceDirect

Energy for Sustainable Development

Operational analysis of hybrid solar/wind microgrids using measured data

Henry Louie

Copperbelt University, P.O. Box 21692, Jambo Drive, Riverside, Kitwe, Zambia

ARTICLE INFO

Article history:
Received 9 October 2015
Accepted 18 January 2016
Available online xxxx

Keywords:
Efficiency
Energy kiosk
Hybrid microgrid
Rural electrification
Solar power
Wind power

ABSTRACT

Microgrids offer a pathway for electricity access to communities located far from the existing grid. Although the simulated operation of microgrids is well-reported in the literature, there is a dearth of analyses based on post-installation high-resolution measured data. This article examines the operation of hybrid solar/wind microgrids using measured data from a 5 kW system in Muhuru Bay, Kenya. The system was outfitted with data acquisition and broadcast equipment that samples battery voltage, current from the solar panels and wind turbines and other quantities on a minutely basis. Considering 14 months of data, this article provides statistical and time-series analyses and interpretation of hybrid solar/wind microgrid operation. The microgrid's energy supply and efficiency are analyzed and data-driven system diagnostic methods are presented. It is shown how microgrid controller set-points influence the prioritization of energy sources, favoring wind over solar energy, and that the long-term efficiency of the microgrid is 67%. Perspectives on how operational data can be used to improve utilization and prevent pre-mature failure are provided.

Introduction

The expansion of centralized grids to serve the 1.1 billion people without electricity is fraught with challenges (International Energy Agency, 2012; Nerini et al., 2014; Alliance for Rural Electrification; Mahapatra and Dasappa, 2012). Low load density and an often impoverished customer base make it difficult to economically justify the extension of distributions lines, which may cost as much as US$20,000 (Alliance for Rural Electrification) per kilometer to install. Constructing and maintaining the lines across rugged terrain coupled with a lack of supporting infrastructure such as roadways add further barriers. In many countries, communities more than 20 km from the grid are not actively considered for electrification by grid extension (Mahapatra and Dasappa, 2012; Japan International Cooperation Agency, 2006; Barfour, 2014). These communities must look to off-grid electrical systems to meet their needs.

The prospects for off-grid systems are promising due to rapidly decreasing component prices and innovative business models. Solar panel prices have plummeted from US$3.17/Wp in 2003 to US$1.15/Wp in 2012 (U.S. Energy Information Administration, 2013). LED bulbs, which are approximately five times more efficient than incandescent lights (U.S. Energy Information Administration, 2014), have also dramatically reduced in price, decreasing from US$66/bulb in 2010 to US$10/bulb in 2014 (U.S. Energy Information Administration, 2014), making the transition from kerosene lamps to electric lighting within reach.

Stand-alone electrical systems serving customers via a local distribution network – hereafter referred to as simply "microgrids" – can supply higher-tiered electricity access when compared with solar home systems or portable battery kits (Sustainable Energy for All, 2015). Research has shown that microgrids, if designed properly, are economically superior to grid extension in many scenarios (Nerini et al., 2014; Alliance for Rural Electrification; Mahapatra and Dasappa, 2012).

Microgrids exist in a variety of architectures, often integrating generation, load, energy storage and protection and control systems. Hybrid microgrids combine two or more energy sources such as photovoltaic (PV) panels, combustion generators, wind turbines and hydro turbines (Nema et al., 2009; Domenech et al., 2014). The most notable advantage of hybrid systems over single-source microgrids is increased security of supply due to the diversification of the energy sources (Nerini et al., 2014; Nema et al., 2009; Domenech et al., 2014). Hybrid solar/wind systems are increasingly being used (Domenech et al., 2014; Nema et al., 2009). They offer the additional benefits of having zero fuel costs and being emission free. However, the operation of hybrid solar/wind microgrids is a complex, as the stochastic load must be matched with the also stochastic weather-driven energy sources (Domenech et al., 2014).

Existing research on the operation and design of hybrid microgrids in general has relied on computer-aided simulation (Alliance for Rural Electrification; Leger, 2015; Ding and Buckeridge, 2000; Bae and Kwasinski, 2012; Valenciaga and Puleston, 2005; Fung et al., 2002). Several innovative control schemes have also been proposed. Use of a multiple input DC–DC converter to manage the sources and loads is used in Bae and Kwasinski (2012). A supervisory control methodology is

E-mail address: hlouie@ieee.org.

http://dx.doi.org/10.1016/j.esd.2016.01.003
0973-0826/

developed in Valenciaga and Puleston (2005). Fuzzy control methods are proposed in Chedid et al. and Yang et al. (2014) and neural network-based control is used in Lin et al. (2011).

Although these methods are innovative, they are not yet commercialized and therefore their use to the practitioner community is limited. Microgrid implementers must use commercially available off-the-shelf products for their immediate needs, yet there is a dearth of literature that analyzes the operation of these in-the-ground systems using measured – not simulated – data. This is unfortunate because operational data can be a powerful tool in validating system performance, maximizing energy production and guarding against premature failure, which haunts many microgrid installations (Tamir et al., 2015; Louie et al., 2014).

Some, but few, analyses that use measured data are available. Data from several off-grid PV installations are considered in Díaz et al. (2011), but these data have only monthly resolution and do not include operational quantities such as voltages and currents. In Tamir et al. (2015), data are provided from post-installation assessment reports but, again, do not include operational data. Higher resolution (10-minutely) operational data are reported in Weber et al. (2014) for a hydroelectric microgrid system. However, Weber et al. (2014)focus exclusively on the load profile of a microgrid. Several researchers have called out the need and value of additional operational data in the research community (Díaz et al., 2011; Cross and Gaunt, 2003; Howells et al., 2002).

This article begins to fill the gap in the literature. Recent advances in cellular network connectivity, cloud-based solutions and measurement hardware have made it possible to obtain near-real time operational data from microgrids (SteamaCo, 2015; PowerHive, 2015; Morningstar Corporation, 2014). Rather than relying on simulation, this paper examines 14 months of data from a 5 kW hybrid solar/wind microgrid in Muhuru Bay, Kenya. The microgrid is outfitted with a data acquisition system that samples battery voltage and branch currents every minute and broadcasts them to a remote server in near-real time. Based on the measured data, this article provides statistical and time-series analyses and interpretation of hybrid solar/wind microgrid operation. The microgrid's energy supply and efficiency are analyzed and data-driven system diagnostic methods are presented.

It is shown how the analyses in this paper were used to maximize the benefit of the microgrid in Muhuru Bay and to prevent premature failure. Although the analyses focus on a specific installation, several of the results are generalizable to hybrid solar/wind microgrids and will be noted as such. For concision, hereafter "hybrid microgrid" specifically refers to solar/wind microgrids.

The remainder of this paper is arranged as follows. The Data and methodology section provides technical information about the microgrid and describes the methodology used to collect and process the data considered in this article. Microgrid control aspects are discussed in the Hybrid microgrid control section. Statistical analyses and time-series interpretation are performed in the Statistical analysis and Time-series analyses sections, respectively. The Microgrid diagnostics section describes a simple diagnostic method for assessing microgrid performance. The efficiency of the microgrid is analyzed in the Efficiency analysis section. Conclusions and future outlook are provided in the Conclusion and future outloook section.

Data and methodology

Microgrid architecture

The data examined in this article are from a hybrid microgrid in Muhuru Bay, Kenya. Muhuru Bay is situated on Lake Victoria, near the border with Tanzania. The system was installed in August 2014 and supplies electricity to the home of a school headmaster and a kiosk where community members can recharge mobile phones, rent portable battery kits and purchase refrigerated beverages and ice. Additional background information about the microgrid, including its community development goals, is found in Van Acker et al. (2014) and Louie et al. (2015).

A high-level schematic of the microgrid architecture is provided in Fig. 1. The architecture and components are typical of solar/wind hybrid microgrids. Wind turbines and PV panels supply power to the system. Two permanent magnet synchronous generator wind turbines harness the strong onshore winds from Lake Victoria. The wind turbines are each rated at 1000 W. The wind turbines output three-phase AC, which is rectified to DC before connecting to the DC bus.

There are twelve 235 W poly-crystalline photovoltaic (PV) panels for a total solar capacity of 2.82 kW. Due to spatial limitations, the PV panels are divided into two sets of six. The natural output of PV panels is DC, so no rectifier is required. Controllers manage the charging of the battery by the PV panels. The controllers play an important and often overlooked role in the operation of the system, which is discussed in detail in the Microgrid diagnostics section. Integrated into each controller is a maximum power point tracker (MPPT). MPPTs increase the power production of PV panels by decoupling their operating voltage from the voltage of the DC bus (Enslin, 1990).

The DC bus voltage is established by the series connection of eight 6 V flooded lead-acid batteries for a nominal voltage of 48 V. Each battery is rated at 400 Ah for a total capacity of 19.2 kWh. Although there are multiple batteries, hereafter they will be referred to as a single unit without loss of specificity.

Also connected to the DC bus is a diversion load controller, which is used to protect the battery from over-voltage conditions. When an over-voltage condition is sensed, a diversion load is connected to the DC bus, thereby reducing the current into the battery and thus lowering the battery's terminal voltage. The diversion load itself is a high-power resistor. It is important to note that the two PV controllers and the diversion load controller are operated autonomously—there are no communication channels between them. Rather, their coordination is achieved solely on the set-points programmed during their installation. This is the reality for many hybrid microgrid systems.

Finally, a single-phase 3000 VA inverter is used to convert DC to AC, which is output to the loads in the house and kiosk. The output voltage is nominally 230 VAC at 50 Hz.

Measurement framework

A data acquisition and broadcast system was integrated into the microgrid. The system measures: total PV current I_{PV}, total wind turbine current I_{WT}, diversion load current I_{DL}, battery terminal voltage V_B, inverter RMS current I_{AC}, inverter RMS voltage V_{AC}, and inverter power factor ψ. Inverter output frequency is also measured but it is not relevant in this article.

The battery current I_B is not directly measured, but it can be computed through the application of Kirchhoff's current law, once all the currents in the branches connected to the DC bus are known. The current into the inverter from the DC bus I_{DC} is also not measured, but it can be reasonably estimated from the measured inverter output quantities as follows. First, the AC power output of the inverter P_{AC} is computed:

$$P_{AC} = V_{AC} I_{AC} \psi. \tag{1}$$

The input power of the inverter P_{DC} is then estimated from:

$$P_{DC} = \frac{P_{AC}}{\eta(P_{AC})} \tag{2}$$

where $\eta(\cdot)$ is the efficiency of the inverter, which is dependent on the AC power output. The assumed efficiency curve of the inverter is provided

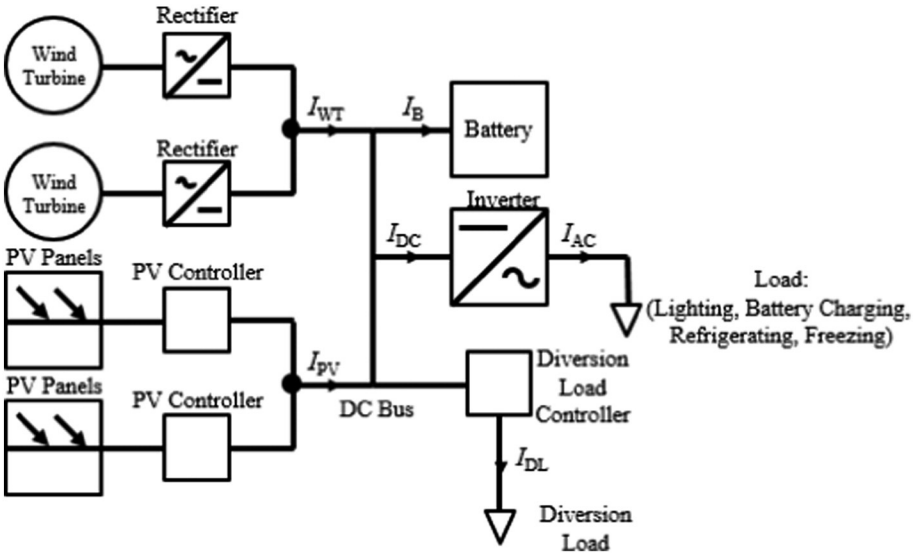

Fig. 1. Schematic of the hybrid microgrid system in Muhuru Bay, Kenya.

in Fig. 2 (Victron). Lastly, the inverter DC input current is computed as:

$$I_{DC} = \frac{P_{DC}}{V_B}. \tag{3}$$

It must be noted that there are losses associated with all of the controllers. Each controller consumes approximately 3 W of power as reported by the manufacturer (Morningstar Corporation, 2014). For simplicity, and without appreciable loss of accuracy, it is assumed that the current into each controller is equal to that out of the controller.

The battery current is computed from Kirchhoff's current law:

$$I_B = I_{WT} + I_{PV} - I_{DL} - I_{DC}. \tag{4}$$

Note that following the formulation in (4), the battery current is positive when charging and negative when discharging.

It is sometimes useful to analyze the performance of the system using power rather current, for example in efficiency calculations. This is done by simply multiplying the branch currents by the DC bus voltage. The bus voltage is assumed to be equal to the battery voltage, which is reasonable due to the low-resistance connection between the bus and the battery. This formulation ignores losses in the wires connecting the equipment, which in practice are negligible.

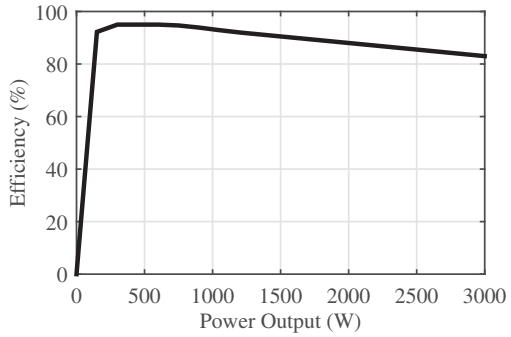

Fig. 2. Assumed efficiency curve of the inverter.

Data acquisition system

An overview of the data acquisition system is shown in Fig. 3. The system nominally acquires the data once per minute and transmits them via a General Packet Radio Service (GPRS) network to a remote server, where the data are archived. The measured quantities are input into the data acquisition system through two analog channels and one Modbus input. The inverter output voltage, current, power factor and frequency use the Modbus input (The Modbus Organization, 2012). The remaining four signals – battery voltage, wind turbine current, solar panel current and diversion load current – are sent to the data acquisition system using time-division multiplexing (Lathi and Ding, 2009).

Time-division multiplexing allows two signals (A and B) to share the same channel. Explained simply, signals A and B take turns being sent through an analog channel so that during one minute signal A is sent, and during the next minute signal B is sent. The disadvantage of this scheme is that the effective sampling rate of each multiplexed signal is decreased to two minutes and that not all values are sampled simultaneously. Battery voltage and wind turbine current share one channel whereas the other channel alternates between PV current and diversion load current.

Data processing

Data irregularities are unavoidable in real-world systems. Over the course of the 14-month period considered, several data irregularities occurred. Although the data were sampled once per minute, the data were not always received by the remote server. The data outages can be classified as intermittent and prolonged. Intermittent outages are caused by several factors, including the SIM card in the system disconnecting from the Kenyan network and "roaming" to the nearby Tanzanian cellular network. Because of the high sampling rate and relatively slow time constants of the system variables, intermittent outages are mitigated by linear interpolation and a five-minute moving average applied to the data set. Prolonged outages occur when the on-site microgrid manager does not reload the SIM card with credit from the mobile network provider in a timely manner.

Over time the sample and broadcast period varied, at times exceeding once per minute. This appears to be due to a hardware irregularity that only affects sampling period, and not the measured values. The

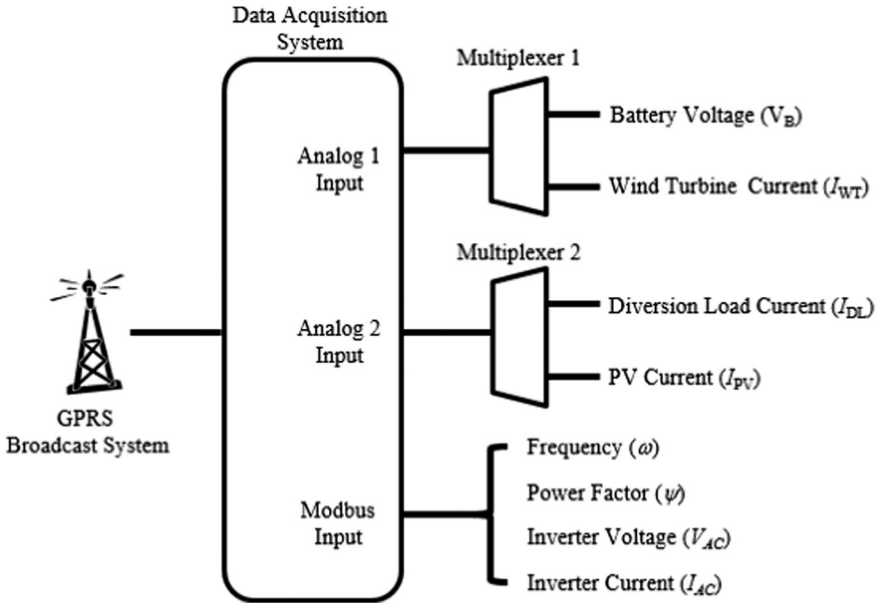

Fig. 3. Schematic of the data acquisition and broadcast system.

statistical analyses that follow only consider days in which at least 60% of the anticipated data were received and with outage durations less than two continuous hours.

Hybrid microgrid control

Hybrid microgrids exhibit a wide range of operational behavior due to the stochasticity of the energy sources and load, as well as the actions of the control and protection systems. Of particular interest, and discussed further in this section, are the PV and diversion load controllers. These controllers influence the charging of the battery and the prioritization of the energy sources. Described hereafter is a generic, yet typical, charge control scheme.

Battery charging

Most lead-acid battery charge controllers use a three-stage charging approach: bulk, absorption and float, as graphically presented in Fig. 4 (Morningstar Corporation, 2012; Victron, 2015). A fourth "equalization" stage is occasionally used for maintenance purposes, but is not considered in this article because it is not part of the routine charging of the battery. The controller begins charging the battery in the bulk stage. The controller maximizes the current into the battery, thus charging it rapidly and raising the battery voltage. The bulk stage ends when the battery voltage reaches the pre-programmed absorption stage voltage set-point. The battery is typically 70 to 80% recharged at the conclusion of the bulk stage.

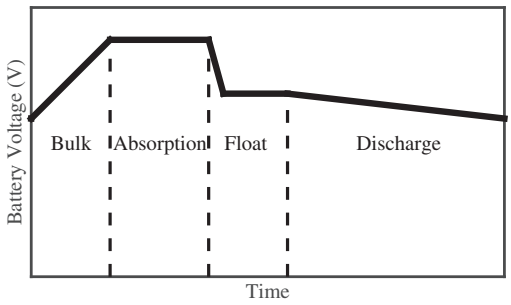

Fig. 4. Charging stages of lead-acid batteries.

Once in the absorption stage, the controller regulates the battery voltage to keep it constant. The battery voltage is a function of the battery's internal voltage V_{int}, which reflects its state of charge, the current into the battery, I_B, and the battery's internal resistance, R_{int}. Although the relationship between these elements is complex (Alber and Migliaro, 1994), for the purposes of this discussion, a simple Thévenin model suffices:

$$V_B = R_{int} \times I_B + V_{int}. \tag{5}$$

For a given state of charge, V_B can be regulated to a specific value by controlling I_B. However, I_B is not controlled directly. Rather, one or more of its constituent components in (4) is controlled, for example the PV or diversion load current. Current control is often achieved using pulse width modulation (PWM) (Krein, 1997). PWM operation can be conceptually thought of as rapidly connecting and disconnecting the source at a controlled duty cycle to achieve a desired time-averaged characteristic.

As the state of charge rises during the absorption stage, the battery current tends to taper off exponentially. Different algorithms exist for determining when to end the absorption phase—some manufacturers use a fixed time, for example four hours, others employ more advanced algorithms (Morningstar Corporation, 2012; Victron, 2015). Regardless, at the end of the absorption stage, the battery is full or nearly-full.

The final stage is the float stage. During this stage, the controller reduces the battery voltage by decreasing the current into the battery to near zero. The goal of the float stage is to simply maintain a full charge on the battery. If the generation sources are unable to supply the load, for example after sunset, then the battery will discharge until adequate generation is available, at which point the bulk stage will begin again.

Table 1
Controller Set-Points

Controller	Absorption (V)	Float (V)
PV	57.6	53.6
Diversion load	58.4	54.8

Controller interaction

The microgrid in Muhuru Bay features three charge controllers, whose set-points are provided in Table 1. The set-points of the two PV controllers are the same and their operation is identical. The diversion load controller set-points are slightly greater than that of the PV controllers. This scheme gives priority to the energy produced by the wind turbines. The reason is as follows. As the battery voltage rises during the bulk stage, the absorption set-point of the PV controllers is reached first. The controller adjusts the PV current so that the battery voltage remains constant at 57.6 V. From Eqs. (5) and (4), in order to keep the battery voltage constant, the PV current must change in response to changes in wind turbine and inverter current. Fig. 5 shows an example of the PV current changing in response to variations in wind turbine current in an attempt to keep the battery voltage constant. As wind turbine current increases, the PV current decreases. This scheme therefore prioritizes wind turbine current.

There are limits to the PV controllers' ability to regulate the battery voltage. Because I_{PV} cannot be negative – this would mean the PV panels are consuming power – high levels of wind turbine current can cause the battery voltage to exceed the PV controllers' absorption set-point. If the voltage reaches 58.4 V, then the diversion controller will enter the absorption stage. The diversion controller regulates the battery voltage by controlling the current into the diversion load I_{DL}, so that less current enters the battery, as dictated by Eq. (4). Should this condition persist long enough, the diversion controller will enter the float stage and will regulate the voltage at 54.8 V.

It may seem strange to include a diversion controller in place of a wind turbine controller. However, it is common practice in hybrid microgrids (Morningstar Corporation, 2012; Hirose and Matsuo, 2011). Reducing current from a wind turbine by disconnecting it from the DC bus as would be done through PWM can cause hazardous and damaging over-speed and over-voltage conditions.

Statistical analyses

The basic operating characteristics of a hybrid microgrid are discerned from profiles of the load (inverter) current, and current from the generation sources, as shown in Fig. 6. For each quantity, the 25th, 50th (median) and 75th percentiles are provided. The percentiles provide information on the variation that occurs. Accompanying statistics are provided in Table 2. Note that the statistics for each variable are computed separately—the median day for solar energy production, for example, does not necessarily correspond to the median day for the load.

The plots of the diversion load current are not shown because they are often zero. However, the diversion load is important for overvoltage protection, and although the median daily energy consumed by it is 80 Wh, it is activated at least once in approximately half of the days.

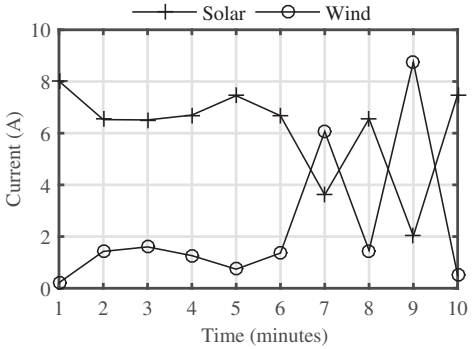

Fig. 5. PV panels and wind turbine current during the absorption stage.

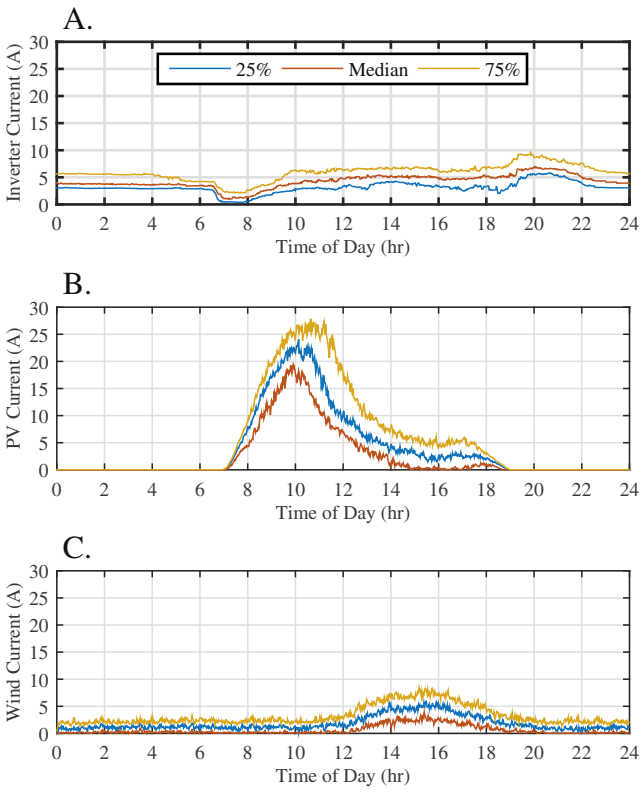

Fig. 6. Quartiles of the microgrid inverter, PV and wind turbine currents.

Fig. 6A shows that the load is generally below 10 A, with the greatest consumption occurring in the evening hours from 19:00 to 22:00, when all of the interior and exterior lights are on, in addition to any overnight charging or refrigeration that might be occurring in the kiosk.

The current from the PV panels is shown in Fig. 6B. As might be expected, the PV panels begin production at sunrise, rapidly increasing until 10:00. Note the large, approximately 10 A difference in production between the 25th and 75th percentiles between 10:00 and 12:00. Also notable is the asymmetry and skewness of the traces. In fact, the 25th percentile trace approaches zero at 15:00, despite the abundance of available solar irradiance at this time. This is caused by the absorption stage operation of the PV controllers and, to a lesser extent, the prioritization of wind energy over solar.

The current from the wind turbines is shown in Fig. 6C. As is common with wind generation, the current follows a diurnal pattern. It peaks around 16:00 and is generally low overnight and in the morning hours. The wind turbines only produce 35% of the energy input to the microgrid. However, this share would be less if not for the controllers prioritizing wind energy over solar energy as described previously.

To further illustrate the variability in energy production that occurs, consider Fig. 7, which shows the energy input by source for a ten-day period of the Muhuru Bay microgrid. It is clear that not only does the absolute amount of production change, but also the relative contribution from each source. This variability is expected in hybrid microgrids in

Table 2
Energy Statistics

Quantity	Min. (kWh)	25% (kWh)	Median (kWh)	75% (kWh)	Max. (kWh)
Load	2.59	4.39	5.30	6.36	10.15
Solar	0.93	3.74	4.80	6.32	10.75
Wind	0.69	2.23	2.84	3.40	7.65
Diversion	0.00	0.03	0.08	0.17	2.05

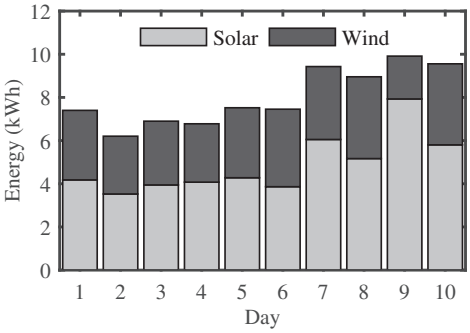

Fig. 7. Energy production by source over a ten-day period.

general. Within the data set are days in which the PV panels produce 90% of the energy, and days in which they produce only 10%.

Time-series analyses

In this section, time-series of three specific days from the data set are examined in detail in order to further elucidate the operation of hybrid microgrids. Proper interpretation of time-series data is important in determining if the microgrid is operating as planned, or is in danger of failure. The time-series correspond to a typical day, a day with high load, and a day with low load but high wind energy production. A qualitative analysis approach is taken, as this is most useful and accessible to microgrid operators reviewing data in real- or near real-time.

Operation under typical conditions

Considered first is a typical operating day, where the load and generation profiles are close to the median values. The specific day is 15 May 2015. Shown in Fig. 8 are the measured battery voltage (V_B); battery current (I_B), load (inverter) current (I_{DC}), PV current (I_{PV}), wind current (I_{WT}) and diversion load current (I_{DL}).

The battery begins the 24-hour period shown in Fig. 8A with a terminal voltage of 49.6 V. The battery is discharging, as evidenced by the negative current at the start of Fig. 8B. The PV current is zero and the wind power is intermittent and near zero. The load is 2.9 A (145 W).

As the sunrises at approximately 7:00, the solar production begins to increase steeply and the load decreases sharply as lighting is switched off. At approximately 7:30, the battery current becomes positive as the PV controllers enter the bulk charging stage. At its peak, the battery is receiving more than 20 A of current (1.1 kW), primarily from the PV panels. The battery current's generally steep rise from 7:00 to 10:45 follows the increase in solar irradiance in the morning hours. The irregularities in the trend are due to intermittent cloud coverage.

The battery voltage rapidly rises during the bulk stage due to the large current, internal impedance of the battery and the increasing state of charge, as in (5). Just before 11:00, the battery voltage reaches approximately 57.6 V—the absorption stage set-point of the PV controllers. The absorption stage lasts until 14:30 as shown in Fig. 8A.

The regulation function of the PV controllers is apparent from the skewness and general asymmetry in Fig 8D. In the absorption stage, the current from the PV panels is being reduced to maintain a constant battery voltage. As the battery's state of charge increases, the current into the battery and from the PV panels decrease in a generally smooth exponential manner beginning just before 11:00 as shown in Fig. 8B and Fig 8D. The PV panels are also supplying the majority of the load current during this time.

The curtailment of solar energy by the PV charge controllers is an important aspect of microgrid operation, and one that can easily be overlooked by designers. In order to realize the production potential of the PV panels load should be added during or shifted to the absorption stage, if possible.

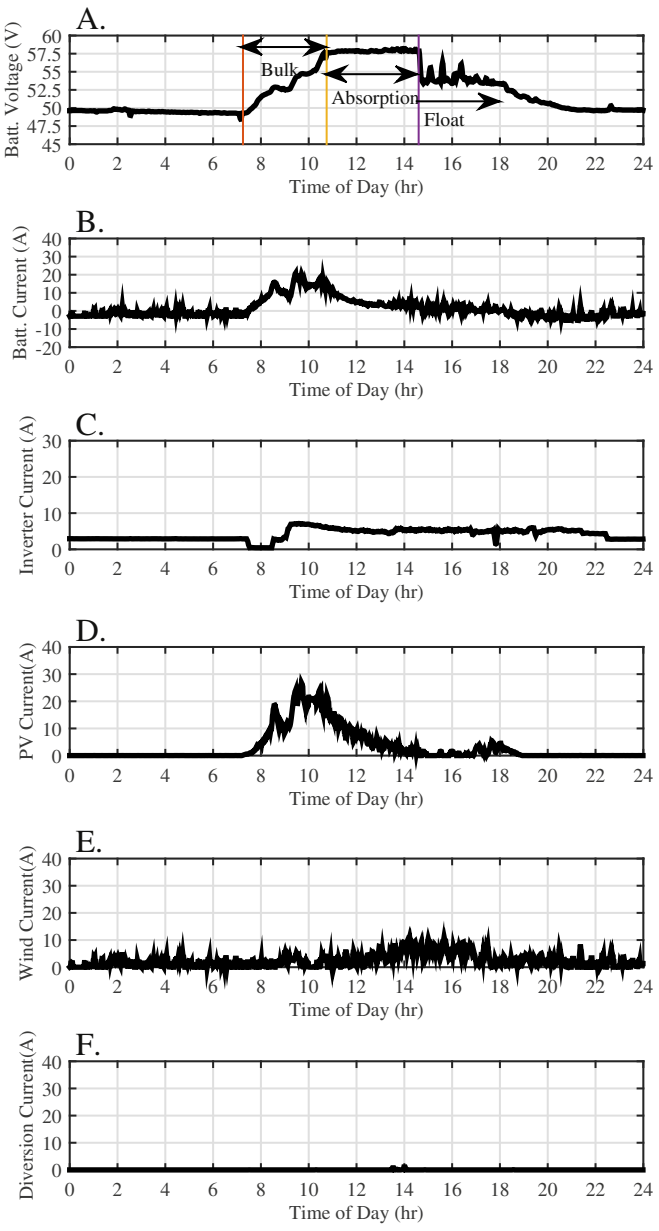

Fig. 8. Time-series of measured quantities for a typical day.

The absorption stage ends at approximately 14:30 and the float stage is entered. The PV current is decreased until a the battery voltage reaches the PV controllers' float set-point (53.6 V). The transient spikes in voltage seen between 15:00 and 17:00 are due to intermittent increases in wind turbine current. The PV current cannot be decreased below zero during these fluctuations and thus the float voltage is not tightly maintained. The diversion controller does not act because the battery voltage remains below its absorption stage set-point.

After 18:30 the battery begins to discharge as the available PV current is insufficient to match the load. The battery voltage is now determined by the load and the wind turbine current. The battery voltage fluctuates during the evening, following the wind power production.

The hallmark signature of the battery voltage rising to the absorption stage set-point, remaining in that stage for several hours and then reducing to the float set-point is a good indicator that the system is operating as designed and that there is sufficient generation to match the load. It is shown next that when demand exceeds the generation, the battery voltage signature is notably different.

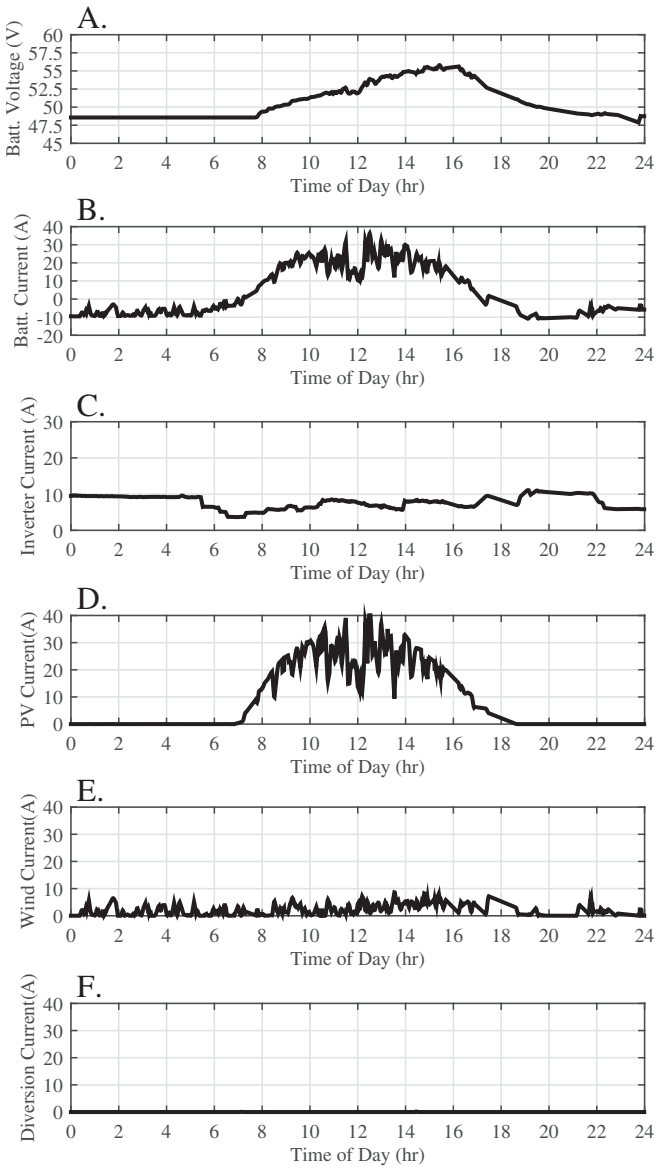

Fig. 9. Time-series of measured quantities for a high load day.

Operation under high load conditions

Considered next is the operation of the hybrid microgrid when the daily load is high. The data correspond to 8 September 2015. A freezer was introduced to the microgrid to sell ice to the fisherman in Muhuru Bay. The profiles are shown in Fig. 9. The load is 8.9 kWh, exceeding the 75th percentile.

The battery begins bulk charging at 8:00 and never reaches the PV controllers' absorption set point voltage of 57.6 V. Also note the profile of PV current in Fig. 9D. The trace is nearly symmetric and the energy production is substantial. The system is maximizing the power produced by the PV panels because the controllers remain in the bulk stage. The PV current is starkly contrasted with the trace in Fig. 8D where it is clearly asymmetric and notably attenuated.

The total production from the PV panels is 11.4 kWh. Although this is greater than the load, it is not enough to overcome losses and a low initial battery state of charge. Because the battery never reaches or completes the absorption stage, it does not obtain a full state of charge. Unless preventative measures are taken, or the wind turbine production increases, the batteries will become discharged to the point that the inverter will self-disconnect and a blackout condition will ensue. After reviewing the profile, the manger of the microgrid was advised to adjust the load by installing more energy efficient lighting and decreasing overnight load. This correction is one example of the usefulness of real-time data monitoring to prevent failure.

Operation under low load/high wind conditions

Next considered is a day with low load and abnormally high wind energy production. The day considered is 7 July 2015. The data corresponding to this day are found in Fig 10. Overnight, a light load of 2.5 A (124.6 W) coupled with a high and consistent wind caused a rare occurrence: the battery was charging before the sun rises, as seen by the generally positive battery current in Fig. 10B and the increase in battery voltage in Fig. 10A during the early morning hours.

At sunrise, the PV controllers begin to bulk charge the battery, but this stage only lasts from 7:00 to 8:30 before the absorption set point voltage of 57.6 V is achieved. The PV current is now being regulated in an attempt to maintain a constant terminal voltage. However, the wind turbine current continues to increase, and after the PV current is

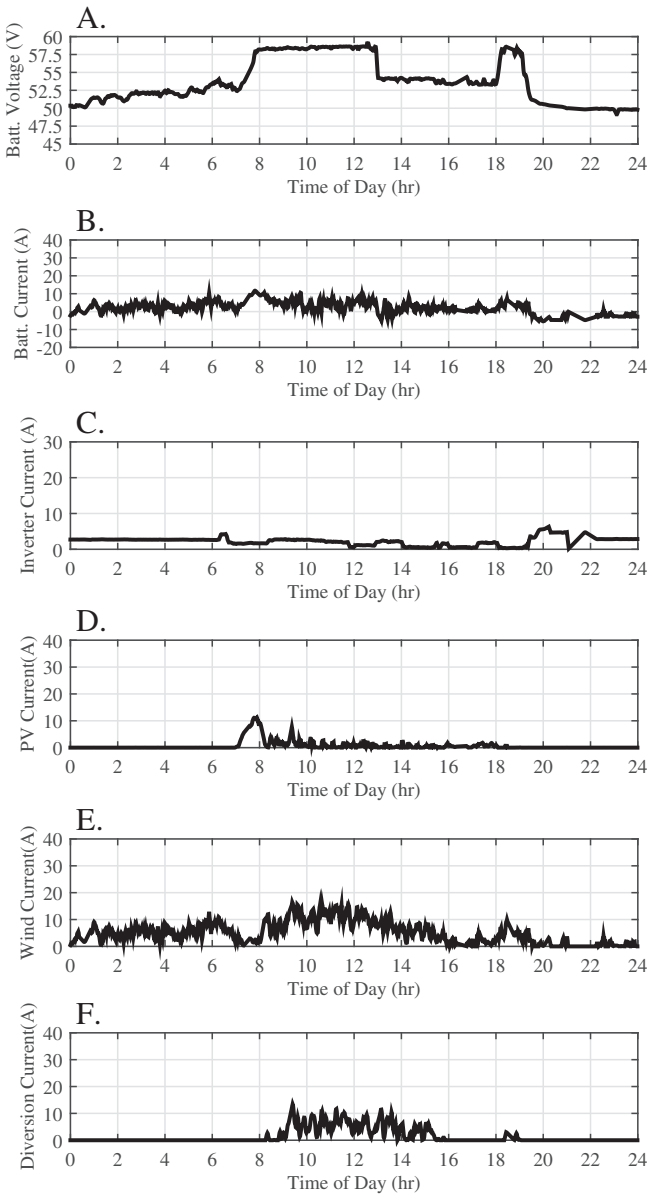

Fig. 10. Time-series of measured quantities for a low load, high wind day.

reduced to zero, the PV controllers can no longer maintain a constant battery voltage. The voltage increases.

The battery terminal voltage reaches 58.4 V — the absorption set-point of the diversion load controller. Inspection of Fig. 10F shows the diversion load current increase from zero starting around 8:30 as the diversion load is activated. The diversion load controller is generally able to maintain the battery voltage at its absorption set-point of 58.4 V.

At 13:00, the absorption stage ends and the voltage decreases sharply to approximately 54.8 V—the diversion controller's float set-point. The battery current vacillates around zero. Inspection of Fig. 10F shows that current is flowing through the diversion load from approximately 8:00 to 16:00, indicating its operation.

The data show another unusual occurrence this day: the appearance of a second spike in voltage from 18:00 to 19:00. By this time the float stage has ended, and the controllers are ready to re-enter the bulk stage. A spike in wind current causes the battery voltage to rise sharply until, again, the absorption set point of the diversion load is reached and the diversion load is briefly activated.

The time-series clearly shows the priority that wind energy is given over solar energy in hybrid microgrids as 6.7 kWh were produced by wind turbines and 0.9 kWh were produced by the PV panels. It also is an example of a day in which it would be technically beneficial to add load to the system to increase solar energy production and utilization. In fact, any time the diversion load is activated, the microgrid operator should consider increasing the load, for example by turning on another refrigerator.

Microgrid diagnostics

It has been shown that the typical operation of a microgrid has the battery's profile distinctly following bulk, absorption and float stage. For off-line monitoring, a straightforward way to determine if the battery is routinely charged is to create a histogram of the battery voltage, as shown in Fig. 11. There should be notable spikes at the absorption set-point and float set-point voltages. Depending on the particularities of the system, other peaks may occur, such as the one around 50 V in the Muhuru Bay system. In general, the absorption stage should last between three and five hours, which is 12 to 16.7% of the hours, as in Fig. 11. Note that some controllers include temperature compensation to automatically adjust voltage set-points, so that the peaks might not exactly correspond to the pre-programmed values.

Additional insight can be gained from examining a histogram of the time at which the absorption stage begins, as in Fig. 12. The start of the absorption stage is detected based on the first sustained (more than 20 min) occurrence of the absorption stage set point voltage in a 24-hour period. The earlier in the day the onset of the absorption stage occurs, the quicker the battery completed bulk stage, indicating either a light overnight discharge or great availability of the solar or wind resource. For Muhuru Bay, the median time that the absorption stage begins is 10:30. Because the wind is more unpredictable and variable, it is important that ample time is given to complete the absorption phase

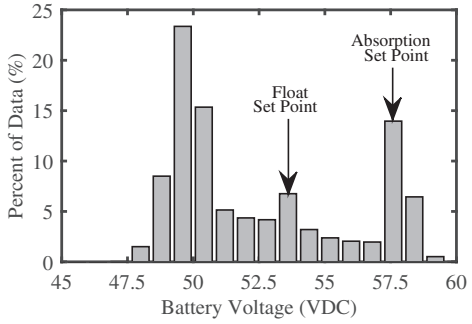

Fig. 11. Distribution of battery terminal voltage.

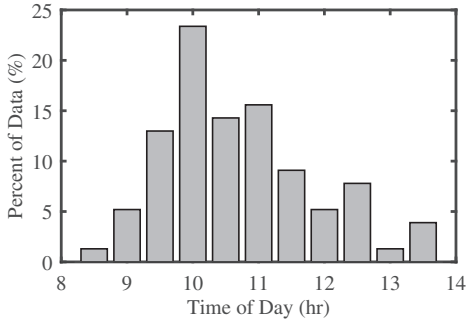

Fig. 12. Distribution of absorption stage starting time.

while there is sufficient solar irradiance. If the absorption stage is reached less than 3 h before sunset, it is likely that the battery is not being fully recharged.

Efficiency analysis

The efficiency of a microgrid is difficult to accurately estimate a priori, yet is critical in designing an appropriately sized microgrid. The efficiency of the microgrid over a 10-day period is shown in Fig. 13. The light grey bars are the sum of the energy produced by the PV panels and the wind turbines. The dark bars are the energy output, which is computed from the inverter output quantities. As expected, due to losses, the daily energy input is greater than the output.

The dashed line in Fig. 13 shows the computed daily efficiency, which ranges from 52 to 74%. The wide variation is strongly influenced by discrepancies in the starting and ending state of charge of the battery. For example, if the battery started the 24-hour period at a low state of charge and ended it with a high state of charge, the apparent efficiency would seem low. Therefore, a more appropriate way to compute the efficiency of the battery is through a multiple day running average, as shown in the solid black line in Fig. 13. The microgrid efficiency stabilizes at approximately 65% during this period, which is comparable to that of the computed lifetime average efficiency of 67%.

The analysis efficiency can be refined further. The chart in Fig. 14 shows how the losses are allocated. The charge controllers are responsible for 8.5% of the losses, based on their reported self-consumption of 3 W. The inverter losses are computed using the curve in Fig. 2, and are responsible for 14.7% of the losses. The diversion load is responsible for 4.0% of the losses. The remaining losses are attributed to the battery

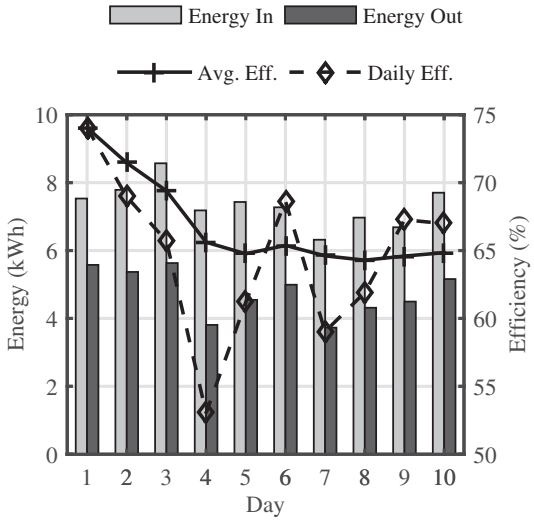

Fig. 13. Energy efficiency of the system over a ten-day period.

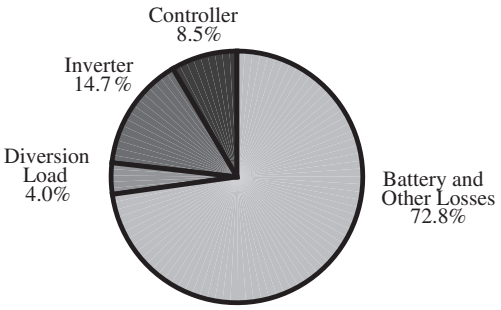

Fig. 14. Share of total losses by component.

and other losses, such as the resistance of the cabling. However, it is expected that these other losses are negligible when compared to the battery losses. The round trip efficiency of the battery is 72.8% or—assuming equal charge/discharge efficiency—a one-way efficiency of 85%.

It is of interest to investigate what conditions make the microgrid more efficient. A strong predictor is the ratio of energy output to total energy exchanged with the battery—either going into or coming from it. This is sensible because energy is lost each time current enters or leaves the battery. Days in which the sum of the energy into and out of the battery are low relative to the overall inverter energy output means that the load temporally corresponds with the energy production, resulting in an efficient system.

Fig. 15 displays a scatter plot of energy efficiency versus energy output divided by total energy exchanged with the battery. The linear correlation coefficient is 0.58, with a p-value of $9.7e-6$, indicating statistical significance. These results support the intuitive guideline that efficient microgrids are those whose demand coincides with the production.

Conclusion and future outlook

Microgrids are an important solutions to electrical energy poverty in rural communities. Analysis of real- or near-real time measured data from microgrids can optimize the usage and prevent against premature failure. This article used minutely-sampled data over a 14-month period to examine how hybrid solar/wind microgrids behave in the field. The article discussed aspects of microgrid control, and showed how controllers influence the operational behavior of the microgrid and prioritization of the energy sources. Statistical and time series analyses were conducted, showing the range of behavior that can exhibited by a hybrid microgrid. Simple diagnostic methods were presented that allow the user to quickly determine if the microgrid is being over- or under-utilized. The efficiency of the microgrid was explored, and it was shown that the microgrid operates at an average efficiency of 67%, with the amount of energy exchanged with the battery relative to the total load being a strong predictor of the efficiency.

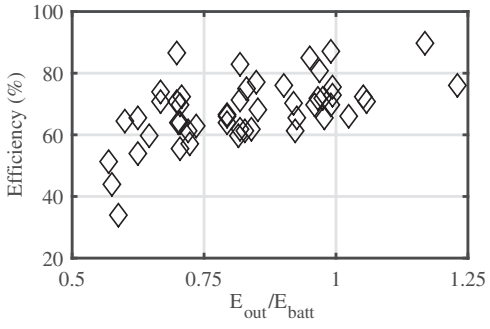

Fig. 15. Scatter plot of the ratio of energy output to energy exchanged with the battery versus microgrid efficiency.

The Muhuru Bay hybrid solar/wind microgrid has produced over 2 MWh of energy to date. Corrective decision-making, informed by the data analyzed in this article, have kept the system on-line and able to continually serve the local community.

This article is the first exploration of the use of high-resolution operational data for microgrid analyses. Future work includes investigating and forecasting microgrid demand, failure analysis and using the data to improve future designs.

Acknowledgment

The author thanks the Alstom Foundation for the Environment and KiloWatts for Humanity.

References

Alber G, Migliaro M. Impedance testing — is it a substitute for capacity tests. Proc. International Telecommunications Energy Conference, Vancouver, BC, Canada; 1994. p. 245–9.
Alliance for Rural Electrification, Hybrid mini-grids for rural electrification, [Online]. Available: http://www.ruralelec.org/38.0.html [Accessed May 2015].
Bae S, Kwasinski A. Dynamic modeling and operation strategy for a microgrid with wind and photovoltaic resources. IEEE Transactions on Smart Grid 2012;3(4):1867–76. http://dx.doi.org/10.1109/TSG.2012.2198498.
Barfour AT. Universal access to energy: Ghana's rural electrification case study. [Online]. Available: http://www.esi-africa.com/wp-content/uploads/i/p/Andrew-Barfour_SmartGrid. pdf, 2014. [Accessed May 2014].
R. Chedid, S. Karaki, C. El-Chamali, Adaptive fuzzy control for wind-diesel weak power systems, IEEE Transactions on Energy Conversion 15 (1) (20).71–78. doi:10.1109/60.849119
Cross N, Gaunt C. Application of rural residential hourly load curves in energy modelling. Proc. IEEE Power Tech Conference, Vol. 3, Bologna, Italy; 2003. p. 1–4. http://dx.doi.org/10.1109/PTC.2003.1304492.
Díaz P, Pena R, Munoz J, Arias C, Sandoval D. Field analysis of solar PV-based collective systems for rural electrification. Energy 2011;36:2509–16. http://dx.doi.org/10.1016/j.energy.2011.01.043.
Ding J, Buckeridge J. Design considerations for a sustainable hybrid energy system. UNITECH Institute of Technology-IPENZ Transactions 2000;27(1):1–5.
Domenech B, Ferrer-Martí L, Lillo P, Pastor R, Chiroque J. A community electrification project: combination of microgrids and household systems fed by wind, PV or microhydro energies according to micro-scale resource evaluation and social constraints. Energy Sustain Dev 2014;23:275–85. http://dx.doi.org/10.1016/j.esd.2014.09.007.
Enslin J. Maximum power point tracking: a cost saving necessity in solar energy systems. Proc. IEEE Industrial Electronics Society Annual Conference, Pacific Grove, CA; 1990. p. 1073–7. http://dx.doi.org/10.1109/IECON.1990.149286.
Fung C, Rattanongphisat W, Nayar C. A simulation study on the economic aspects of hybrid energy systems for remote islands in Thailand. Proc. IEEE Region 10 Conference on Computers, Communications, Control and Power Engineering, Beijing, China; 2002. p. 1966–9. http://dx.doi.org/10.1109/TENCON.2002.1182724.
Hirose T, Matsuo H. Standalone hybrid wind-solar power generation system applying dump power control without dump load. IEEE Transactions on Industrial Electronics 2011;59(2):988–97. http://dx.doi.org/10.1109/TIE.2011.2159692.
Howells M, Alfstad T, Cross N, Jeftha L, Goldstein G. Rural energy modeling. [Online]. Available: http://www.erc.uct.ac.za/Research/publications-pre2004/02Howells-etal_Rural_Energy_Modelling.pdf, 2002. [Accessed Oct 2015, Oct].
International Energy Agency. World energy outlook 2012. [Online]. Available http://www.iea.org/publications/, 2012. [Accessed Oct. 2015].
Japan International Cooperation Agency. Cambodia master plan study on rural electrification by renewable energy in kingdom of Cambodia. [Online]. Available: https://www.climate-eval.org/sites/default/files/evaluations/190, 2006. [Accessed Oct. 2014, Feb.].
Krein P. Elements of power electronics. Oxford, UK: Oxford University Press; 1997.
Lathi B, Ding Z. Modern digital and analog communication systems. 4th ed. Oxford, UK: Oxford University Press; 2009.
Leger AS. Demand response impacts on off-grid hybrid photovoltaic-diesel generator microgrids. AIMS Energy 2015;3(201503360):360–76. http://dx.doi.org/10.3934/energy.2015.3.360.
Lin W, Hong C, Chen C. Neural-network-based MPPT control of a stand-alone hybrid power generation system. IEEE Transactions on Power Electronics 2011;26(12):3571–81. http://dx.doi.org/10.1109/TPEL.2011.2161775.
Louie H, Dauenhauer P, Wilson M, Mutale J, Zomers A. Eternal light: Ingredients for sustainable off-grid energy development. Power & Energy Magazine 2014;12(3):70–8. http://dx.doi.org/10.1109/MPE.2014.2317093.
Louie H, O'Grady E, Acker VV, Szablya S, Kumar N, Podmore R. Rural off-grid electricity service in Sub-Saharan Africa. IEEE Electrification Magazine, 3 (1). ; 2015. p. 7–15.
Mahapatra S, Dasappa S. Rural electrification: optimising the choice between decentralised renewable energy sources and grid extension. Energy Sustain Dev 2012;16:146–54. http://dx.doi.org/10.1016/j.esd.2012.01.006.

Morningstar Corporation. Tristar three-function solar controller. [Online]. Available: http://www.morningstarcorp.com/wp-content/uploads/2014/02/TS.IOM_.Operators_Manual.04.EN_.pdf, 2012. [Accessed Oct 2015, Apr.].
Morningstar Corporation. Tristar mppt. [Online]. Available: http://www.morningstarcorp.com/wp-content/uploads/2014/02/TSMPPTdsEng.pdf, 2014. [Accessed Oct 2015].
Nema P, Nema R, Rangnekar S. A current and future state of art development of hybrid energy system using wind and PV-solar: a review. Renew Sustain Energy Rev 2009; 13:2096–103. http://dx.doi.org/10.1016/j.rser.2008.10.006.
Nerini F, Howells M, Bazilian M, Gomez MF. Rural electrification options in Brazilian Amazon a multi-criteria analysis. Energy Sustain Dev 2014;20:36–48. http://dx.doi.org/10.1016/j.esd.2014.02.005.
PowerHive T. [Online]. Available: http://www.powerhive.com/our-technology/, 2015. [Accessed Oct 2015].
SteamaCo. Off-grid monitoring tools. [Online]. Available: https://steama.co/, 2015. [Accessed Oct 2015].
Sustainable Energy for All. Progress toward sustainable energy. [Online]. Available: http://www.se4all.org/wp-content/uploads/2013/09/GTF_2015-Summary_Report.pdf, 2015. [Accessed Oct. 2014].
Tamir K, Urmee T, Pryor T. Issues of small scale renewable energy systems installed in rural Soum centres in Mongolia. Energy Sustain Dev 2015;27:1–9. http://dx.doi.org/10.1016/j.esd.2015.04.002.
The Modbus Organization. Modbus application protocol specification. [Online]. Available: http://www.modbus.org/docs/Modbus_Application_Protocol_V1_1b3.pdf, 2012. [Accessed Oct 2015, Apr.].
U.S. Energy Information Administration. Solar photovoltaic cell/module shipments report. [Online]. Available: http://www.eia.gov/renewable/annual/solar_photo/, 2013. [Accessed Oct. 2015, Dec.].
U.S. Energy Information Administration. Annual energy outlook. [Online]. Available: http://www.eia.gov/forecasts/AEO/pdf/0383, 2014. [Accessed Jan. 2015, Apr.].
Valenciaga F, Puleston P. Supervisor control for a stand-alone hybrid generation system using wind and photovoltaic energy. IEEE Transactions on Energy Conversion 2005; 20(2):398–405. http://dx.doi.org/10.1109/TEC.2005.845524.
Van Acker V, Szablya S, Louie H, Sloughter J, Pirbhai A. Survey of energy use and costs in rural Kenya for community microgrid business model development. Proc. IEEE Global Humanitarian Technology Conference, Seattle, WA; 2014. p. 166–73.
Victron. Bluesolar charge controller MPPT 150/70. [Online]. Available: http://www.victronenergy.com/, 2015. [Accessed Oct 2015[.
Victron, Technical notes on output rating, operating temperature and efficiency, [Online]. Available: http://www.victronenergy.com/TechnicalInfo/TechPDF/Output (Accessed Jun 2015).
Weber K, Kennedy S, Armstrong P. End-use load monitoring of a micro hydroelectric-powered community microgrid: a case study in rural Malaysia. Proc. Innovating Energy Access for Remote Areas, Berkeley, CA; 2014. p. 23–5.
Yang J, Cheng K, Wu J, Dong P, Wang B. The study of the energy management system based-on fuzzy control for distributed hybrid wind-solar power system. Proc. IEEE Power Electronics Systems and Applications, Hong Kong; 2014. p. 113–7. http://dx.doi.org/10.1109/IECON.1990.149286.